

Arbitrary Waveform Generated Metasurface: A New Paradigm for Direct Modulation and Beamforming Decoupling

Xuehui Dong, Bokai Lai, Rujing Xiong, Jianan Zhang, Miyu Feng, Tiebin Mi, Robert Caiming Qiu

Abstract—Passive arbitrary waveform generation (AWG) are especially important in a variety of fields like radar detection, wireless communications and integrated sensing and communications. Typically, backscatter devices are used to achieve passive signal reflection modulation to facilitate information transmission or to interfere with radar echoes. Reconfigurable Intelligent Surface (RIS) or Metasurface is a promising technology that combines the advantages of backscatter devices and reflective array antennas. Previous studies demonstrate diverse approaches to achieve reflection modulation by utilizing the superposition of the quantified reflective coefficient (RC) of each unit but suffer from the computing complexity of codebook sequence, the safety of communication, and the flexibility of modulation. To overcome the difficulties, we propose new paradigm of metasurface, i.e. AWG-RIS, that can independently generate arbitrary baseband waveforms and beam patterns based on a magnitude-phase decoupled unit design without altering the beam pattern. We proposed an analysis framework and introduce waveform factor and beamforming factor into the new model which provide the theoretical support for the flow from the control signal to the outgoing electromagnetic wave. Furthermore, we introduce the world's first prototype that demonstrates passive arbitrary waveform generation without altering the beam pattern. The experiments validate the generation of arbitrary waveforms and spectrograms, both for a single input and through the superposition of multiple inputs.

Index Terms—Reconfigurable Intelligent Surfaces, waveform generation, AWG-RIS, reflection modulation, direct modulation, backscatter communication, radar spoofing.

I. INTRODUCTION

Metasurfaces, comprised of 2D arrays of sub-wavelength units, have attracted great attention because of their remarkable capabilities in manipulating electromagnetic (EM) wave. The generality of the manipulation is the superposition of effect of each unit, which could be the variation of reflective coefficient (RC), polarization and spectrum etc. [1], [2], [3]. The emerged reconfigurable intelligent surface (RIS) or information metasurface focuses on dynamically changing its EM characteristics, thereby encoding the information on the EM wave. Most work on RIS consisting of patch antennas and diodes or variodes concatenates the digital signal and quantized EM characteristics (e.g., RC) for the achievement of reconfigurability. However, there are some critical disadvantages about the existing researches of programable information metasurface.

Xuehui Dong, Bokai Lai, Rujing Xiong, Jianan Zhang, Miyu Feng, Tiebin Mi, Robert Caiming Qiu are with School of Electronic Information and Communication, Huazhong University of Science and Technology, Wuhan 430074, China (e-mail: xuehuidong@hust.edu.cn; bokailai@hust.edu.cn; rujing@hust.edu.cn; zhangjn@hust.edu.cn; feng-miyu@hust.edu.cn; mitiebin@hust.edu.cn; caiming@hust.edu.cn)

National Foundation (NSFC), NO.12141107 supports this work.

In modern communication theory, information is modulated in the carriers due to the convenience of the spatial transmission and the receiving by the compact antenna. The principle of modulation of the transmitter is that the baseband signal is shifted on the carriers by the mixer. However, the baseband signal generated by RIS comes from manipulating the EM characteristics of each unit using a digital control signal.

A. Prior work

Research on information metasurfaces can be broadly categorized into three aspects: spatial coding, temporal coding, and spatial-temporal coding. The spatial coding works on the dimension of physical space, which manipulates near-field distribution and far-fields scattering or radiation of EM wave [4]. Different fields distribution and radiation pattern represent different symbols.

The concept of temporal coding has been proposed that manipulates the spectrum of the reflected EM wave while the RC of the metasurface periodically varies [5]. This concept evolves applications such as nonlinear harmonic frequency manipulation [5], independent control of magnitude and phase of the harmonic frequency [6], efficient frequency synthesis [7], multiple polarization transformation [8], nonlinear convolution computing [9] and also the wireless communication transmitter [10], [11], [12]. However, the temporal coding does not take into account the energy distribution of the reflected EM wave.

To tackle this issue, the spatial-temporal coding theory framework in terms of metasurface is proposed [13]. That simultaneously manipulates the spatial energy distribution and the spectral distribution of the reflected EM wave through the jointly encoding of discrete RCs in the time domain and the space domain [14], [15], [16]. This coding approach has been applied in the fields of harmonic beam switching and beamforming [13], multibit phase generation [17], Doppler and spectral cloak [18], radio frequency (RF) computing [19], wireless communication [20], [21], [22], cognitive radar [23], generation of orbital angular momentum (OAM) [24], [25], RF imaging [26], etc.

Many studies have improved the conventional RIS structure from a different perspective. Active-RIS, which includes active reflection-type amplifiers, alleviates the persistent multiplicative fading issue associated with passive RIS, providing a notable advantage in SNR [27], [28], [29], [30]. Both STAR-RIS (Simultaneous Transmitting and Reflecting RIS) [31], [32] and TS-RIS (Tri-State RIS) [33], [34] address the topological constraints of reflecting-only RIS by incorporating new meta-atom designs with specific bias voltages

or currents, enabling STAR-RIS to achieve greater diversity gain and TS-RIS to function as an absorbing layer, thus diversifying the roles of RIS. Some works have proposed and designed anisotropic metasurfaces that are independently programmable in real-time for orthogonal polarized waves [35], [36].

B. Deficiency of existing work

Many current studies indicate that the baseband signal is typically produced by implementing a specific sequence of beam patterns, resulting in a coupling of information and the beam pattern. This introduces three significant and unavoidable challenges:

- **The computing complexity of the codebook sequence:** Due to coupling, simultaneously accommodating both beamforming and signal generation functions results in excessively high computational complexity for codebook sequences in real-time tasks.
- **The physical layer security and intercept probability:** Because the main lobe energy of the beam cannot always point towards the target receiver (as spatial-temporal coding requires a varying main lobe to generate the signal), targets in other directions can detect the same pattern of variation, thus compromising the physical layer security and the intercept probability.
- **Arbitrary waveform generation:** Due to discrete EM characteristics and digital signal control, RISs cannot generate continuous baseband signals. This limitation makes RISs less practical in many fields compared to some backscatter devices [37], [38].

To overcome the challenges, it is essential to decouple the baseband signal generation and the beamforming functionality in RIS. Let us consider a similar technology that meets this requirement: the multiple inputs multiple outputs (MIMO) transmitter. The capability to radiate electromagnetic waves in specific directions is provided by the phase shifters and power allocator on each antenna in the RF front end [39]. Meanwhile, the process of generating baseband signals involves the DAC generated baseband signal being mixed onto the carrier produced by the local oscillator through non-linear devices, forming the carrier envelope [40].

Remark 1. *The key to decoupling the baseband signal from the beamforming mode lies in the ability to independently control the magnitude and phase of the reflection coefficients of RIS units. The variation in the magnitude of the reflection coefficients affects the envelope of the outgoing electromagnetic waves, while the distribution of phase within the array forms specific beamforming patterns.*

The key issue is how to achieve low-cost continuous control of the unit's RC. In fact, previous studies have already explored methods for continuous control of reflection coefficients. Fusco, etc. applied dc bias control to the equivalent distributed Schottky diode, thereby direct amplitude modulation of a CW microwave carrier can be achieved [41]. Some reflection amplifiers [42] have also been considered to provide continuous and arbitrary values of RC, such as the tunneling diode [43], the varactor diode [44], and the junction-gate field-effect transistor (JFET) [45]. The signal processing module controls the voltage output of the biasing

source, which alters the effective impedance of the amplifier and thus the parameters of the backscatter signal [37].

C. Main contributions

To address the deficiency of existing work, we consider a 1-bit patch antenna RIS with one PIN diode, and propose a new paradigm of RIS, i.e. AWG-RIS, which decoupled the arbitrary baseband waveform generation and beamforming functionality with a low-cost and novel structure. Our main contributions are summarized as follows:

- We propose the AWG-RIS that has a decouple-oriented unit design and a functionality-separated control structure. In particular, the magnitude of the well-designed unit RC can be continuously manipulated by the analogue control signal with a stationary phase while the PIN diode is conducting. Utilizing the analog switches, the analog control of waveform generation and the digital control of beamforming can be separated into individual module that has different performance in accordance with the practical demand. The AWG-RIS can independently generate arbitrary continuous waveforms and beam patterns.
- We propose an analytical framework and introduce two factors into the AWG-RIS model which provide theoretical support for the flow from the control signal to the reflected EM wave. The impulse response of the control circuit and the non-linear characteristic of the diode represent the limitation and distortion of the reflective baseband signal compared to the input signal. New dimension has been developed by the introducing of the independent waveform factor in new model. We also defined the modulation efficiency of AWG-RIS.
- Using the proposed new paradigm and analysis framework, we present the world's first prototype that implements passive arbitrary waveform generation by RIS. In our prototype, the AWG-RIS has 1-bit quantization of phase and eight inputs of the control signal. The prototype validates the decoupled functions of waveform generation and beamforming. With different numbers of inputs, the prototype can generate arbitrary waveform in diverse way such as single-input direct generation, and multi-input superimposed generation. On this basis, we discuss the future prospects of the AWG-RIS in certain fields and present several primary demonstrations.

D. Organization

The reminder of this paper is organized as follows. In Section II, we deconstruct and reconstruct the RIS, including the control circuits and the patch antenna, and illustrate the physical principle of the new paradigm RIS. In Section III, we present the structure and model of the AWG-RIS, and look ahead the promising application of it. In Section IV, we demonstrate the approaches of arbitrary waveform generation with single input and waveform synthesis with multiple inputs. The prototype of AWG-RIS and the validation of arbitrary waveform and spectrum generation are presented in Section V. Finally, Section VI concludes the paper.

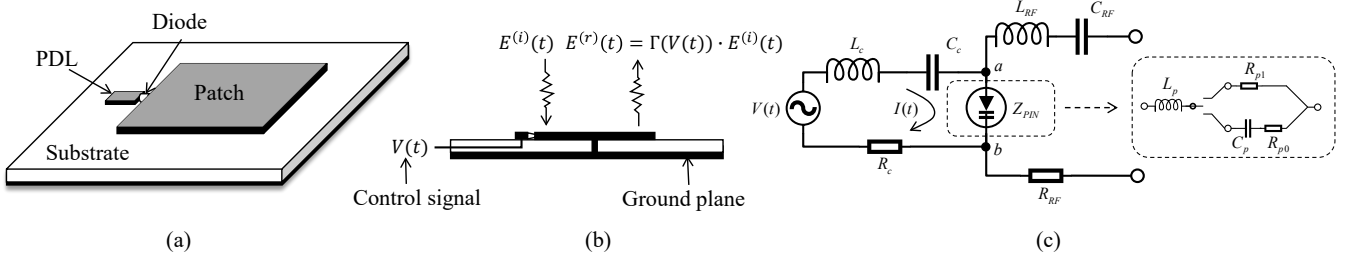


Figure 1. (a) A normal 1-bit unit of RIS consists of ground plane, substrate, patch, phase delay line (PDL) and diodes; (b) A sketch of the side view: the reflective coefficient of unit depends on the control signal $V(t)$; (c) Equivalent circuits of both controlling part and RF part.

II. DECONSTRUCTION AND RECONSTRUCTION OF RIS

In this section, we proposed an framework which can continuously manipulate the magnitude of the reflective coefficient (RC) with an invariable phase. First, we model the unit of RIS including the controlling circuits in order to derive the formulation of RC. The magnitude-phase decoupled approach is obtained by utilizing the nonlinearity of the PIN diode, different equivalent resistance values at different bias voltages. The reflected baseband signal is controlled simultaneously by RIS while the beam pattern remains stationary. We focus on the regular structure of the unit as shown in Fig.1 (a). Prior researches on metasurface mostly focus on the digital functionality of PIN diodes, which have two states: ON and OFF. Based on different structures, the combinations of PIN diodes in unit comprise the set of several discrete RCs $\{\Gamma_i\}$, $i = 1, 2, \dots, L$. The consistent philosophy designing the metasurface's unit is that, keeping the magnitude of RCs of the set as high as possible and the phase is evenly distributed.

When RIS is used as an information metasurface, its ability to control EM waves should be utilized to encode information into the outgoing EM waves. It is preferable to modulate more variations onto the emitted EM waves to improve information transmission. The baseband signal is produced by varying a carefully designed temporal sequence of beam patterns, known as a codebook sequence, referred to as temporal-spatial coding. However, for information modulators, this method involves a concession because it cannot separately manage the beam and the baseband signal. Consequently, the modulation function and the beamforming function are coupled. To enhance modulation flexibility, an innovative RIS design is necessary that separates these two functions.

A. Reflective Coefficient of Unit

The integrated equivalent circuits of unit including the controlling part and the RF part is shown in Fig.1 (c). Earlier studies primarily focus on the RF component, as the control segment is reduced to a simple 0/1 digital signal input. Bit 0/1 corresponds to a fixed input value V_0 which makes the voltage V_{ab} across the PIN diode a voltage less or large than the forward conduction voltage $V_{forward}$. The efficient impedance can be expressed as

$$Z_{eff}(\omega) = Z_{PIN} + R_{RF} + j\omega L_{RF} + \frac{1}{j\omega C_{RF}}, \quad (1)$$

where Z_{PIN} is the equivalent impedance of PIN diode as

$$Z_{PIN} = \begin{cases} R_{p0} + j\omega L_p + \frac{1}{j\omega C_p} & , V_{ab} = V_0 \\ R_{p1} + j\omega L_p & , V_{ab} = V_1 \end{cases}. \quad (2)$$

Combining with equation (1), we can obtain the expression of RC when the PIN is in forward bias

$$\begin{aligned} \Gamma(V_{ab} = V_1) &= \frac{Z_{eff}(\omega) - Z_0}{Z_{eff}(\omega) + Z_0} \\ &= \frac{R_{p1} + R_{RF} + j\omega(L_{RF} + L_p) + \frac{1}{j\omega C_{RF}} - Z_0}{R_{p1} + R_{RF} + j\omega(L_{RF} + L_p) + \frac{1}{j\omega C_{RF}} + Z_0} \\ &= A_1 e^{j\omega\phi_1}, \end{aligned} \quad (3)$$

where $Z_0 = 377\Omega$ is the impedance of free space, and A_1 and ϕ_1 is respectively the magnitude and phase of RC when the bias voltage of PIN diode is V_1 . Similarly, $\Gamma(V_{ab} = V_0) = A_0 e^{j\omega\phi_0}$.

B. Non-linearity of PIN diode and Response of RLC circuit

A PIN diode operates in two modes: forward and zero-bias. This traditional perspective has limited us to the use of digital signals to control RIS.

The PIN diode is inherently nonlinear. This nonlinearity is apparent not only in its different behaviors under forward and zero-bias conditions but also in the non-linear relationship between current and voltage during forward bias operation. In other words, the equivalent impedance of the PIN diode varies with the bias voltage across its terminals even in the forward state. The relationship between the voltage V_{ab} across the PIN diode and its equivalent impedance Z_{PIN} can be described by a characteristic function $Z_{PIN} = p(V_{ab})$. In conjunction with Eq.(3), we know that, through the application of carefully crafted continuous analog signals to control RIS units made up of PIN diodes, the reflection coefficient of the unit can be adjusted in a continuous manner.

In practice, the voltage across the diode is not exactly equal to the control voltage. As shown in Fig.1, the control circuit can be regarded as an RLC (Resistor Inductor Capacitor) circuit, where $V_{ab}(t)$ and $V(t)$ exhibit not only scaling, but also temporal dispersion (frequency selectivity in the spectrum domain). A specific RLC control circuit will cause a certain degree of distortion in the control waveform. We can define a time-invariant impulse response $h_{cc}(t)$ for the control circuit, which accurately represents the relationship

between the control signal and the voltage across the diode, i.e.,

$$V_{ab}(t) = \int_0^t h_{cc}(\tau)V(\tau - t)d\tau. \quad (4)$$

So that the relationship between control signal $V(t)$ and equivalent impedance Z_{PIN} , while the PIN diode is forward conducting, is

$$Z_{PIN}(t) = p \left(\int_0^t h_{cc}(\tau)V(\tau - t)d\tau \right). \quad (5)$$

The design of $h_{cc}(t)$ is crucial in applications where RIS is used to generate waveforms. We utilize circuit theory to optimize the control circuit, aiming to meet the following two requirements to ensure that the control circuit's signal is efficiently and undistortedly reflected across the diode's terminals: (a) The transfer function $H_{cc}(\omega)$ remains as constant as possible over the baseband signal range; (b) $|H_{cc}(\omega)|$ should be as high as possible.

In summary, the accurate reflection of the control signal in the baseband signal requires the combined effect of the control circuit, the characteristic function of the PIN diode, and the design of the unit patch.

C. Decoupling the Magnitude and Phase of Reflective Coefficient

To achieve a higher degree of freedom of modulation (DoF), allowing continuous control of the baseband signal while maintaining the beam pattern, our aim is to decouple the magnitude and phase of RC of the RIS unit. We utilize the fact that the PIN diode's high-frequency resistance is inversely proportional to the DC bias current through the diode. A suitably biased PIN diode therefore acts as a variable resistor. The wide intrinsic region also means the diode will have a low capacitance when zero-biased.

This implies that the RC of the unit is a piecewise function w.r.t. $V_{ab}(t)$. When the diode has zero bias, the reflection coefficient is a stable constant $\Gamma(V_{ab}(t) < V_{forward}) = A_0 e^{j\omega\phi_0}$. When the diode is forward conducting, the magnitude of RC becomes $\mathcal{L}\{V_{ab}(t)\}$, while the phase of RC ϕ_1 remains constant and unaffected by the control voltage. It can be expressed as

$$\begin{bmatrix} A(t) \\ \psi(t) \end{bmatrix} = \begin{cases} \begin{bmatrix} \mathcal{L}\{V_{ab}(t)\} & \phi_1 \end{bmatrix}^T, & V_{ab}(t) \geq V_{forward} \\ \begin{bmatrix} \alpha & \phi_0 \end{bmatrix}^T, & V_{ab}(t) < V_{forward} \end{cases}, \quad (6)$$

where the projection $\mathcal{L}\{\cdot\}$ is strictly monotone increasing and injective, $A(t)$ and $\psi(t)$ are respectively the magnitude and phase of RC at time t , $V_{forward}$ is the forward conducting voltage, α is the magnitude of RC when the diode is zero bias. Usually, $\mathcal{L}\{V_{ab}(t)\} < \alpha$ for all $V_{ab}(t)$.

According to Eq.(1), we learn that the varying resistance values of the PIN diode under different bias voltages affect both the magnitude and phase of the reflection coefficient simultaneously. It is necessary to choose an appropriate structure and a set of parameters for the unit of RIS if we need to keep the phase of RC constant under different bias voltages. As shown in Fig.2, a combination of rectangular patch and PDL was selected, with specific design details referenced from our previous work [46].

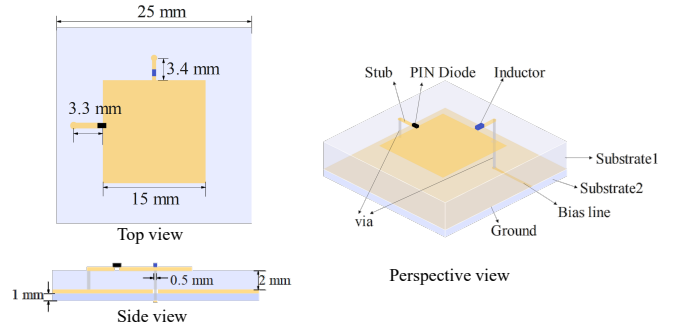


Figure 2. The three views of the geometry of unit with stub.

The phase difference is mainly decided by the switching of the PDL. The RC's magnitude difference depends on the equivalent resistance of the PIN diode. As shown in Fig.3, we set different equivalent resistances for the components that represent the diode in CST studio, resulting in the magnitude and phase of the RC of the RIS unit at different voltages. The 1D result shows that the magnitude of RC continuously decreases as V_{ab} approaches $V_{forward}$. Equivalently, the larger resistance corresponds to the lower magnitude of RC while PIN diode is conducting. In the mean time, the phase of RC remains almost unchanged.

Remark 2. Based on well-designed units such as Fig.3 and Eq.(6), the magnitude and phase of RC are decoupled. The variation of magnitudes contributes to the waveform generation and the superposition of phases constitutes the beam pattern.

Here, an important parameter, the minimum magnitude of the reflection coefficient $|\Gamma|_{min}$, largely determines the ability to generate waveforms. $|\Gamma|_{min}$ is related to the modulation efficiency η of amplitude modulation (AM), which reflects the power distribution between the carrier signal and the information signal. When the incident wave power is fixed, a higher η enhances the noise immunity of the baseband waveform generated by the RIS. It is shown that the η of the unit designed by us is around 25%. Higher modulation efficiency can be achieved by further optimizing the unit structure, circuit design, and the type of diodes used, or even by utilizing transistors. It is found that a high equivalent resistance could reduce the value of $|\Gamma|_{min}$ due to the approach to the impedance of the free space Z_0 based on Eq.(3). So, the SMP1345-079LF PIN diode in our unit design could be replaced by another diode with higher resistance.

Assuming we already obtain the mapping operator $\mathcal{L}\{\cdot\}$ from the voltage across the diode to the magnitude of the reflection coefficient when the PIN diode is forward biased, the equivalent impulse response of the control circuit $h_{cc}(t)$ and the control signal $V(t)$, then

$$|E^{(r)}(t)| = \mathcal{L}\{h_{cc}(t) * V(t)\} \cdot |E^{(i)}(t)|, \quad (7)$$

where $|E^{(r)}(t)|$ and $|E^{(i)}(t)|$ are respectively the magnitude of reflected wave and incident wave, $*$ denotes convolution operator.

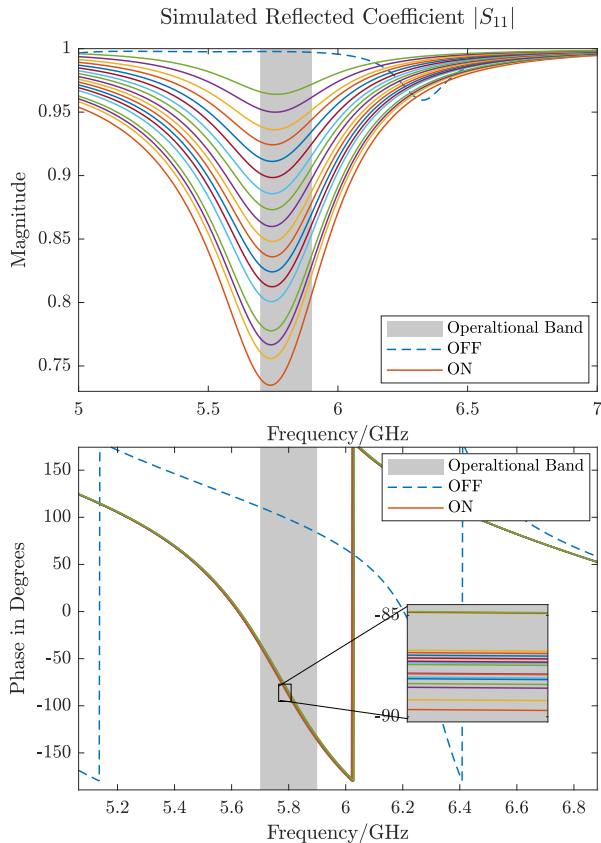


Figure 3. The 1D simulated results of S_{11} , i.e., Reflective Coefficients $\Gamma(\omega)$ from CST studio. The upper sub-figure illustrates the magnitude $|S_{11}|$ of unit under different bias-voltage. The lower one illustrates the phase $\angle S_{11}$ under different bias-voltage. The solid lines represent characteristics when the PIN diode is conducting, i.e., ON state. The dash line represents characteristic when the cross voltage is zero, i.e., OFF state.

D. Decoupling Waveform Generation and Beamforming

Considering a RIS-aided wireless radio channel, the received signal strength is not only depends on the RC of each unit of RIS but also the superposition of all the outgoing wave. In traditional active array antenna transceiver, the beamforming function is achieved through the combined use of phase shifters and power allocators, while the baseband signal is input directly by the feed source. Most reflection modulation works generate the corresponding baseband waveform by utilizing variation of the beam pattern. This is because the magnitude and phase of the reflection coefficient are coupled, significantly reducing the DoF of reflection modulation.

Based on the concept and design of decoupling the magnitude and phase of RC described in the previous section, we could easily decoupling the functions of waveform generation and beamforming on RIS. Given a certain beam pattern and a arbitrary waveform, we generally follow two steps:

- 1) Determining the discrete phase shift codebook according to the given beam pattern;
- 2) Calculating the control signal of all the PIN diodes, which are in ON state, according to the given waveform.

Those PIN diodes in OFF state keep a constant magnitude α of RC, which do not disturb the generated baseband

waveform except for the superposition modulation efficiency.

In practical applications and actual design implementations, the phase exhibits minimal jitter, typically within a range of 5° , as illustrated in Fig.3. Due to the quantification of the phase shift, such an error is negligible for a directional beam, as shown in Fig.4. In this result, the directions of the main lobe would not change when the ON-state PIN diodes are biased by different voltages.

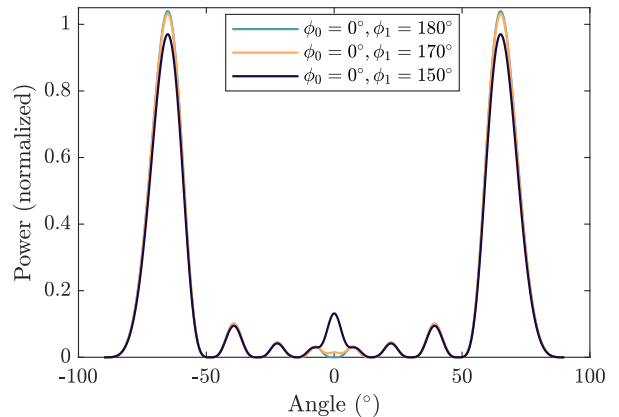


Figure 4. Comparison of beam patterns for diode phase deviations of 10° and 30° from the reference of 180° in the ON state. Simulation setting: a uniform linear array 1-bit RIS with 16 units, 5.8GHz center frequency; normal incident plane wave, approximately 60-degree angle of departure.

III. NEW PARADIGM OF AWG-RIS

In the preceding section, we expounded on the utilization of analog signals to govern specifically designed RIS units comprising 1-bit PIN diodes, facilitating continuous amplitude modulation while preserving the near-constant phase of the RC. This innovation heralds a distinct separation between RIS beamforming and modulation functionalities. Through the introduction of analog signal control, we advocate for a pioneering paradigm shift in RIS technology.

A. The Structure of AWG-RIS

The new paradigm of metasurface decouples the modulation and beamforming functionalities. Each functionality has different performance requirements in different application scenarios. For example, in scenarios aimed at enhancing signals for mobile terminals, beam tracking requires faster beam pattern switching speeds. Conversely, when serving as transmitters (backscatter communication devices), higher sampling rates are demanded from the signal generator's digital-to-analog converter (DAC). Modulation and beamforming functionalities require control of analog and digital signals, respectively. Therefore, we propose a novel decoupled control approach for RIS, as illustrated in Fig.6.

Within the most general framework, we consider the output of the i th analog switch (AS) as the control signal $V_i(t)$ of each unit, with each analog switch's output determined by a digital enable signal $b_i(t)$ and an analog waveform signal $x_j(t)$ from the j th DAC, i.e.,

$$\begin{aligned} V_i(t) &= b_i(t) \cdot x_j(t), \\ b_i(t) &\in \{0, 1\}, x_j(t) > V_{forward}, \end{aligned} \quad (8)$$

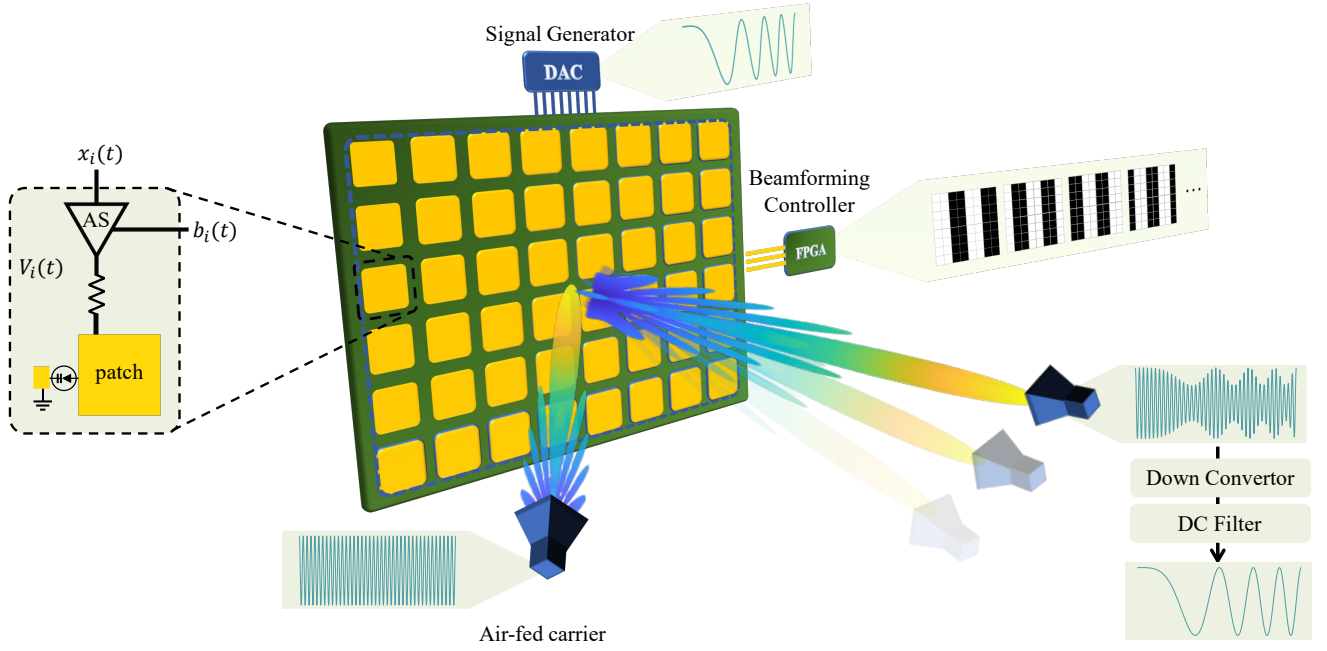


Figure 5. Conceptual illustration of the independent implements of arbitrary waveform generation and beamforming using the AWG-RIS. The decoupled unit design and the functionality-separated control structure enable more flexible and promising RIS applications. Through the combined regulation of the analog control signal $x_i(t)$ and the digital enable $b_i(t)$ of each unit, the RIS is capable of direct and continuous reflection modulation concerning the incident EM wave without altering the beam pattern. The beamforming controller's codebook sequences can effortlessly direct the primary lobe of the beam pattern towards the target in real-time, leaving minimal energy in other directions.

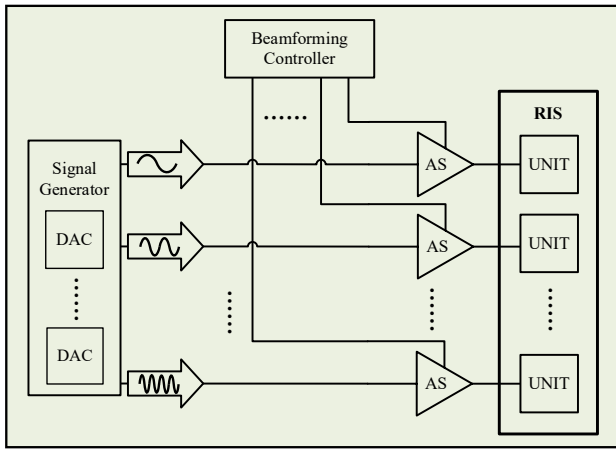


Figure 6. The structure of control part of AWG-RIS.

where N , M are respectively denoted as the number of units and DACs. $i = 1, \dots, N$, $j = 1, \dots, M$. The enable signal actually corresponds to the state of PIN where 0 and 1 are equivalent to OFF and ON. The diagonal matrix $\mathbf{B}(t) = \text{diag}\{b_1(t), b_2(t), \dots, b_N(t)\}$ is actually the digital codebook of the traditional RIS control framework. The correspondence between $V_i(t)$ and $x_j(t)$ can be represented using a discrete mapping $\mathcal{P} : i \rightarrow j$.

In practice, the number M of DACs depends on demand in different scenarios, which is much less than the number N of units. Also, DACs could be replaced by certain waveform generated circuits that are cheap and practical. We distinguish

between signal generation and beamforming functionalities at the hardware level, enabling more flexible allocation of hardware resources according to specific requirements.

B. The Model of AWG-RIS

The traditional RIS model is no longer applicable to systems with the new hardware architecture. Considering that the amplitude and phase of the unit's RC are decoupled, the unit model can be expressed as

$$\begin{aligned} E^{(r)}(t, z_k) &= \Gamma_k(t) E^{(i)}(t, z_k) \\ &= A_k(t) e^{j\psi_k(t)} E^{(i)}(t, z_k), \end{aligned} \quad (9)$$

where z_k represents the coordinate of k th unit, $A_k(t)$ and $\psi_k(t)$ is respectively the magnitude and phase of k th unit's RC $\Gamma_k(t)$ at t moment. Based on Eq.(8) and Eq.(7), we obtain the definitions of magnitude and phase of RC with respect to beamforming controller module and signal generator module:

$$A_k(t) = \mathcal{L}\{h_{cc}(t) * x_j(t)\} \cdot b_k(t) + \alpha \cdot (1 - b_k(t)), \quad (10a)$$

$$\psi_k(t) = \phi_1 \cdot b_k(t) + \phi_0 \cdot (1 - b_k(t)), \quad (10b)$$

where ϕ_0 and ϕ_1 denote the phases at diode state OFF and ON.

Considering a point at position z outside the RIS array, to simplify the model and highlight the effect of the reflection coefficient, we neglect specific path losses. Thus, the electric field at that point is the linear superposition of the reflected waves from each unit. The electric field $E^{(r)}(t, z)$ at position z can be expressed as:

$$E^{(r)}(t, z) = \sum_{k=1}^N A_k(t) e^{j\psi_k(t)} e^{j\frac{2\pi}{\lambda}|z-z_k|} E^{(i)}(t, z_k). \quad (11)$$

According to remark 2 and the new structure, we introduce two factor representing the separated functionalities, waveform generation and beamforming:

$$\mathbf{A}(t) = \begin{bmatrix} A_1(t) & & & \\ & A_2(t) & & \\ & & \ddots & \\ & & & A_N(t) \end{bmatrix}, \quad (12a)$$

$$\mathbf{\Psi}(t) = \begin{bmatrix} e^{j\psi_1(t)} & & & \\ & e^{j\psi_2(t)} & & \\ & & \ddots & \\ & & & e^{j\psi_N(t)} \end{bmatrix}, \quad (12b)$$

where $\mathbf{A}(t)$ is the waveform factor and $\mathbf{\Psi}(t)$ is the beamforming factor, $A_k(t)$ and $\psi_k(t)$ are defined in Eq.(10). The introduction of separated waveform factors and beamforming factor enhances the flexibility of RIS functionalities.

Assuming both the incident and reflected waves are under far-field conditions, when considering a SISO system composed of an AWG-RIS with a feed signal of monochromatic wave at angular frequency ω_0 , the received electromagnetic wave can be modeled as:

$$E^{(r)}(t) = \sum_{k=1}^N A_k(t) e^{j(\omega_0 t + \phi_{init} - \theta_k^{(r)} + \theta_k^{(i)} + \psi_k(t))}, \quad (13)$$

where ϕ_{init} represents the initial phase of incident EM wave, $\theta_k^{(i)}$ and $\theta_k^{(r)}$ denote the relative phase corresponding to the steering vectors of incident \mathbf{e}^* (θ^i) and reflected wave \mathbf{e}^* (θ^r). The matrix form of Eq.(13) can be expressed as

$$E^{(r)}(t) = \mathbf{e}^*(\theta^r) \mathbf{A}(t) \mathbf{\Psi}(t) \mathbf{e}(\theta^i) e^{j(\omega_0 t + \phi_0)}, \quad (14)$$

We respectively define two sets with respect to indices of zero-biased and conducting units,

$$\begin{aligned} B_0 &= \{k | b_k = 0, \forall k = 1, \dots, N\}, \\ B_1 &= \{k | b_k = 1, \forall k = 1, \dots, N\}. \end{aligned} \quad (15)$$

These two sets are complementary to each other, i.e., $B_0^c = B_1$. According to the workflow described in section.II.D, these two sets B_0 and B_1 are defined once a specific beam pattern is provided, as well $\mathbf{B}(t)$ and $\mathbf{\Psi}(t)$. [47] gave the conclusions that the beam pattern will not change when the phase shift of each unit gains the same increment. For a 1-bit RIS, given a specific beam pattern, there always exists a codebook $\mathbf{B}(t)$ such that the set B_1 contains more than $N/2$ elements.

Now we analyze the received baseband signal $y(t)$ under the assumption of Eq.(13),

$$\begin{aligned} y(t) &= E^{(r)}(t) \cdot e^{-j\omega_0 t} + n(t) \\ &= \sum_{k=1}^N A_k(t) e^{j(\phi_{init} - \theta_k^{(r)} + \theta_k^{(i)} + \psi_k(t))} + n(t), \end{aligned} \quad (16)$$

where $n(t)$ is additional white Gaussian noise (AWGN). We use the beamforming gain G_b to represent the strength gain caused by the antenna phase compensation. The Eq.(16) can be simplified as

$$y(t) = G_b \sum_{k=1}^N A_k(t) + n(t). \quad (17)$$

The above equation is a reasonable approximation under two condition: (a) the baseband signal bandwidth is much smaller than the center frequency; (b) the aperture size is much smaller than the minimum wavelength of the baseband signal. Based on Eq.(6), the $A_k(t)$, $k \in B_1$ would have modulate the waveform into the EM wave, rather than the $A_k(t)$, $k \in B_0$ that have the constant RC. This implies that the cumulative modulation efficiency $\eta_m(t)$ will actually fluctuate with changes in the beam pattern,

$$\eta_m(t) = \frac{\sum_{k \in B_1} \|A_k^{ac}(t)\|_2}{\sum_{k \in B_1} \|A_k(t)\|_2 + \sum_{k \in B_0} \alpha^2}, \quad (18)$$

where $A_k(t)$, $k \in B_1$ is separated as the ac part $A_k^{ac}(t)$, $k \in B_1$ and the dc part $A_k^{dc}(t)$, $k \in B_1$. The η_m affects only the power of the signal carrying the information, not the waveform itself. The dc part of signal is normally filtered by the band-pass filter in receiver. Therefore, we introduce a modulation attenuation factor L_m ,

$$y(t) = L_m G_b \sum_{k \in B_1} A_k^{ac}(t) + n(t). \quad (19)$$

where $A_k^{ac}(t) = A_k(t) - \int_{T_0}^{T_0 + \Delta T} A_k(\tau) d\tau$, and ΔT is the length of a symbol.

C. New Potential of AWG-RIS

Remark 3. Compared to traditional RIS, the AWG-RIS introduces an additional dimension of operation, specifically the waveform of the baseband signal.

This additional dimension can be realized by introducing a few economical DACs. The capability of waveform generation extends the potential of RIS, making it more versatile for applications in various fields.

1) *Backscatter Communication:* The number and accuracy of available RCs in an impedance-matching network determine the communication capability of the backscatter tag. Traditional impedance networks can only support a discrete and limited number of RCs. Typically, Backscatter Communication and RIS serve different application purposes: Backscatter Communication is primarily used for data delivery with low energy consumption, while RIS is mainly employed to enhance communication performance in a passive manner [37].

However, the AWG-RIS supports not only continuous control of RCs but also independent manipulating beam patterns. On the one hand, compared to traditional backscatter devices, beamforming maximizes the signal-to-noise ratio at the receiver. Compared to previous work on RIS modulation, the capability of waveform generation allows for the transmission of information at the highest data rate using arbitrary modulation techniques.

As shown in Fig.7, the beamforming controller is FPGA and signal generator is DAC module. Fig.7.(a) shows that the FPGA only responds for the simultaneous user tracking and the DAC responds for the baseband signal. The computing complexity greatly decreases because the baseband signal is not generated through the variation of beam pattern; Fig.7.(b) shows that the beam pattern with multiple main lobes can serve a multi-user broadcast channel; Fig.7.(c) shows that the beamforming sequence and baseband symbols are jointly

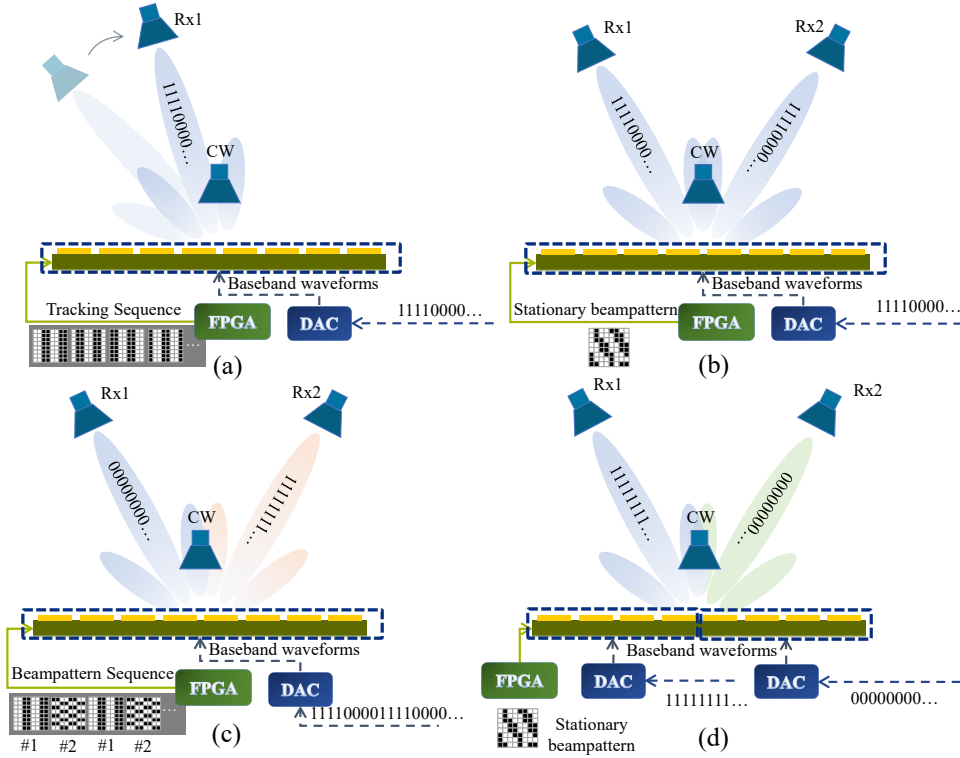


Figure 7. Some use cases in terms of backscatter communication with the AWG-RIS. (a) Mobile receiver scenario;(b) Multi-user broadcast scenario;(c) Time-division multiplexing scenario;(d) MIMO-like transmitter scenario;

designed to achieve time-division multiplexing transmission. Fig.7.(d) shows that the AWG-RIS with two DACs is similar to the MIMO transmitter with two antennas.

2) *Radar Spoofing*: Arbitrary waveform generation is equivalent to arbitrary time-frequency signature generation, as shown in Fig.15. The AWG-RIS have the ability to imitate objects with any motion pattern that manifests in the micro-Doppler signature. For radars focused on velocity estimation, RIS mounted on object surfaces can deceive the detector by shaping the baseband waveform. Due to its independent control over both the baseband signal and the beamforming pattern, its proficiency in broadband signal modulation significantly surpasses that of conventional RIS.

3) *Integrated Sensing and Communication (ISAC)*: The AWG-RIS is suitable for the radar-centric communication. The RIS mounted on the object to be detected can embed the communication waveforms into the incident radar waveforms as an envelope. Some of the desired random signals will be remodulated into the deterministic waveform in a form that maintains the necessary sensing performance, as shown in Fig.8. The capability of direct reflection modulation without changing the beam patterns offers an intriguing method to achieve radar-centric communication with greater flexibility.

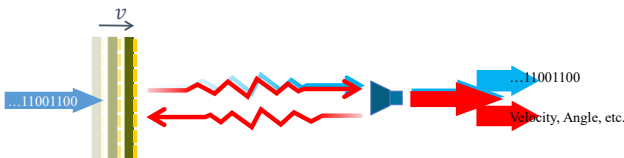


Figure 8. The AWG-RIS assisted radar-centric communication scheme.

IV. ARBITRARY WAVEFORM GENERATION BY AWG-RIS

This section will introduce how to generate an arbitrary waveform with different numbers of DACs in this new paradigm.

A. Waveform Generated with Single Input

We hope that the outgoing wave has a baseband signal with the waveform $y(t)$, neglecting the dc part. Assuming there is single input, that is, $V_i(t) = x_1(t), \forall i \in B_1$, each conducting unit's magnitude of RC can be derived based on Eq.(7). We obtain the output of DAC $x(t)$ by

$$x(t) = \mathcal{L}^{-1}\{y(t)\} * h_{cc}^{-1}(t), \quad (20)$$

where the \mathcal{L}^{-1} denotes the inverse projection of \mathcal{L} and the $h_{cc}^{-1}(t) * h_{cc}(t) = 1$. Theoretically, it is enough for RIS to generate arbitrary waveform by only a single input such as DAC. The workflow that how to generate an arbitrary waveform under a specific beam pattern is described in algorithm 1.

Algorithm 1 Arbitrary waveform generated by single-input RIS with new structure described in Section III.A

Require:

- $\mathcal{L}\{\cdot\}$: the projection from $V_{ab}(t)$ to $|\Gamma|$,
- $h_{cc}(t)$: the impulse response of control circuit,
- $F(\omega)$: the beam pattern during a symbol.

Ensure: Arbitrary Baseband Signal $y(t)$.

- 1: obtain the codebook $\mathbf{B}(t)$ from $F(\omega)$ by certain beam-forming algorithm
- 2: calculate the input signal $x(t)$ by (20)
- 3: **return**

Nevertheless, generating a baseband signal with a wide bandwidth using a single input is practically challenging due to the band-pass characteristics of the control circuits' transfer function $H_{cc}(\omega)$. A wideband signal requires a high-bandwidth DAC and a high-performance digital signal processor (DSP), both of which are expensive. This predicament could be tackled by the superposition principle and the reconstruction of waveform.

B. Time-frequency Waveform Generation with Multiple Input

The superposition principle derived from Maxwell's equations forms the foundation of all signal analysis theories. Based on the expression of the baseband signal in Eq.(19), the waveform can be composed by different components with distinct features such as frequency. In order to tackle with the problem mentioned in the previous sections, it is feasible for generating a wide band signal by designing units' control circuits with distinct pass-bands and integrating them into the RIS.

Time-frequency analysis is the theory that studies the signal whose frequency content changes over time. The short-time Fourier transform (STFT) is a Fourier-related transform that is used to determine the sinusoidal frequency and phase content of local sections of a signal as it changes over time. Conversely, the inverse STFT can also produce a wideband signal composed of multiple frequency components within the corresponding time segment.

Assuming that we have a real wideband baseband signal $y(t)$, due to the symmetry of the spectrum, its frequency range is $[-B/2, B/2]$. This signal is considered to be combined by K narrow-band inputs. The symbol length of $y(t)$ is T_m , and the sample rate of signal generator is F_s which is much larger than $2B$ as the Nyquist's theorem. So we get a discretized version $y[n], n = 1, \dots, N_m$, where $N_m = \lfloor T_m/F_s \rfloor$. So the discrete STFT $\mathbf{Y} \in \mathbb{C}^{L \times M}$ of $\mathbf{y} \in \mathbb{C}^{N_m \times 1}$ can be expressed as

$$\mathbf{Y} = \Xi_L \mathbf{W}_t \mathcal{H}_{L,M}(\mathbf{y}) \quad (21)$$

where m is the frame index, l is the frequency bin index, H is the hop size, L is the point of discrete Fourier transform (DFT) and $M = \lfloor \frac{N_m}{H} \rfloor$. $\Xi_L \in \mathbb{C}^{L \times L}$ is a DFT matrix with a primitive L th root of unity $e^{-j2\pi/L}$. $\mathbf{W}_t \in \mathbb{R}^{L \times L}$ is the window diagonal matrix with the corresponding value of windows in the diagonal line such as Hamming windows. $\mathcal{H}_{L,M}(\cdot)$ is the generalized Hankel matrix transform which can reshape a $N_m \times 1$ vector to a $L \times M$ matrix. The DFT matrix Ξ_L is defined by

$$\Xi_L = \frac{1}{\sqrt{L}} \begin{bmatrix} 1 & 1 & 1 & \dots & 1 \\ 1 & \omega & \omega^2 & \dots & \omega^{L-1} \\ 1 & \omega^2 & \omega^4 & \dots & \omega^{2(L-1)} \\ 1 & \omega^3 & \omega^6 & \dots & \omega^{3(L-1)} \\ \vdots & \vdots & \vdots & \ddots & \vdots \\ 1 & \omega^{L-1} & \omega^{2(L-1)} & \dots & \omega^{(L-1)(L-1)} \end{bmatrix} \quad (22)$$

where the $\omega = e^{-j\frac{2\pi}{L}}$.

The normal hamming windows diagonal matrix $\mathbf{W}_t = \text{diag}\{\mathbf{w}_t\}$,

$$\mathbf{w}_t[n] = a_0 + (1 - a_0) \cos\left[\frac{2\pi n}{L}\right], \quad n \in [L/2, L/2]. \quad (23)$$

where $a_0 = \frac{25}{46}$.

The generalized Hankel transform $\mathbf{B} = \mathcal{H}_{L,M}(\mathbf{b})$ is define as

$$\{\mathbf{B}\}_{i,j} = \mathbf{b}[i + (j - 1)H], \quad (24)$$

where $\mathbf{B} \in \mathbb{R}^{L \times M}$, $\mathbf{b} \in \mathbb{R}^{N_m \times 1}$.

The matrix \mathbf{Y} represents the signal spectrogram \mathbf{y} , where the j th column of \mathbf{Y} denotes the spectrum in the j th time slot. The i th row denotes the i th frequency bin of the signal. The bandwidth represented by a frequency bin can be calculated by $\Delta B = B/L$. Assuming there are K nonoverlapping narrow-band inputs, we can express the spectral window diagonal matrix as

$$\mathbf{W}_\Omega = \sum_{i \in \Omega} \mathbf{W}_i, \quad (25)$$

where $\mathbf{W}_i \in \mathbb{R}^{L \times L}$ has a 1 at the i -th diagonal position, with all other elements being 0. The set Ω has the same frequency bin indices as the corresponding input in terms of rows in \mathbf{Y} . The corresponding frequency bins can be selected by $\mathbf{W}_\Omega \mathbf{Y}$.

Algorithm 2 STFT based multi-input RIS waveform synthetic

Require: \mathbf{y} : Original Signal, K : Number of inputs, Ω_k : Set of the frequency bins of k th input.

Ensure: Waveform of each input.

- 1: obtain the spectral window \mathbf{W}_{Ω_k} by (25)
 - 2: calculate the spectrogram \mathbf{Y} by (21)
 - 3: **for all** i such that $1 \leq k \leq K$ **do**
 - 4: obtain the masked spectrogram by $\mathbf{Y}_k = \mathbf{W}_{\Omega_k} \mathbf{Y}$
 - 5: calculate the inverse STFT \mathbf{y}_k
 - 6: calculate the control signal of each input $x_k(t)$ by (20)
 - 7: **end for**
 - 8: **return** $x_k(t), \forall k$
-

The Algorithm 2 demonstrates the process of creating a wide-band waveform by dividing it into multiple narrow-band components using discrete STFT.

V. EXPERIMENTAL VALIDATION & PROTOTYPE

A. Prototype

We present the prototype setup of wireless passive arbitrary waveform generation system based on RIS here, which illustrates the hardware design and architecture, including the AWG-RIS prototype and the detailed hardware modules and their roles in the prototype system. The prototype system realizes passive waveform generation with single input, superimposed waveform generation with multiple inputs, and arbitrary spectrogram synthesis over the air. The experimental results demonstrate the feasibility of our proposed paradigm of RIS that decouple the baseband signal and beam pattern.

B. Prototype Setup

1) *AWG-RIS*: We designed and produced a 10×16 -unit 1-bit RIS with 8 signal-input SMA-interfaces (i.e., 1#~8#) which works at the operating frequency of 5.8GHz, as shown in Fig.10. The upper interfaces is for the digital enable signal $b_i(t)$ from FPGA, which controls the beam pattern of reflected EM wave. The analog switch (MAX4597) is in ON

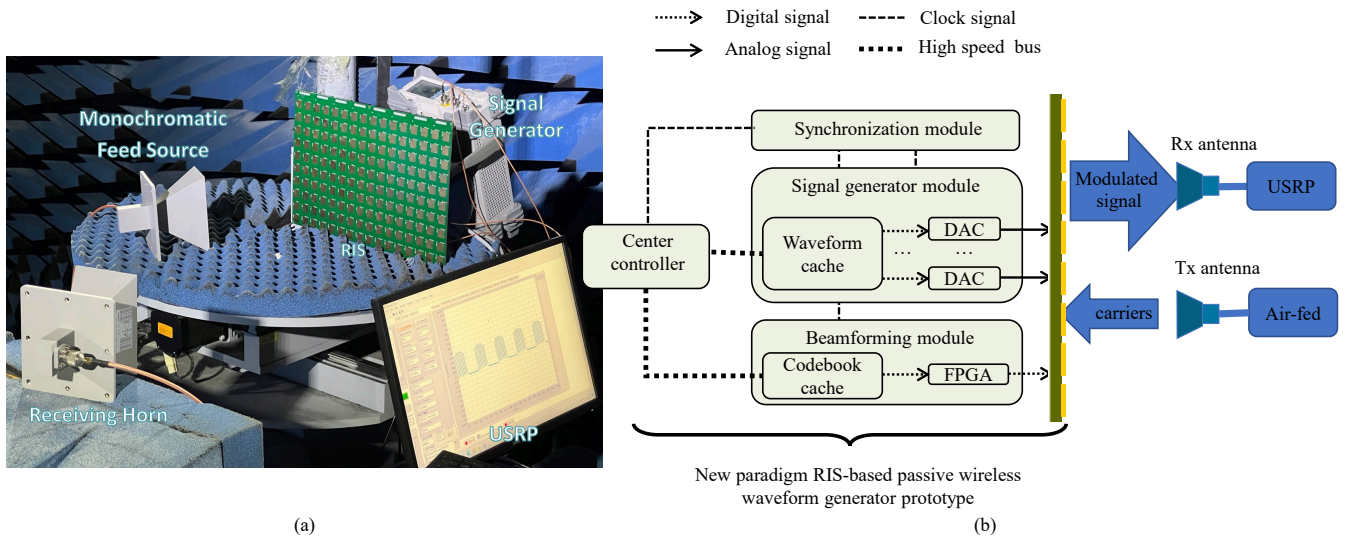


Figure 9. The experimental validation of the proposed waveform generation using AWG-RIS. (a) A photo of the experimental scenario; (b) The schematic of the prototype's architecture.

state while the enable voltage is low, the verse is high. The SMA-interfaces on the bottom are the inputs of analog control signal $V_i(t)$ which responds for the manipulation of the RC's magnitude of each unit so that the baseband signal can be modulated on the reflected EM wave. Each SMA-interface is connected with two nearby columns of units. Within the radiated unit cell, the main metallic patch is connected to the bias line, that is, the output of the AS. To eliminate interference, a choke inductor (LQW15AN19NG00D) is incorporated to isolate the current from the RF signal. The adjacent edge of the patch is connected to the ground through a stub. The stub consists of a specially designed PDL and a PIN diode (SMP1345-079LF), which has a stable equivalent inductance of 0.7 nH and a variant equivalent resistance from tens of ohms to minuteness while the input voltage increases from 700 mV. It is equivalent to a capacitance of 1.8 pF in series with a 0.7nH inductor if the input voltage is less than 700 mV.

2) *Signal Generator Module*: The signal generator module consists of a waveform cache and multiple DACs. The cache holds the digital data regarding the waveform, provided by the center controller. The center controller ensures that the cache sends the digital data to the appropriate DACs in synchronization with the external clock signal. The DACs then generate the desired waveform into the control circuits as shown in Fig.1.(c). As indicated in Section III.A, the DACs can be substituted with various types of waveform generation circuits.

3) *Beamforming Module*: The beamforming module consists of a codebook cache and an FPGA. Each FPGA output supplies the enable signal to the AS. High voltage indicates an open state between the output and input of the AS, whereas low voltage indicates a short state. Codebooks for each departure angle could be pre-stored in the cache when the relative position of the air-fed source is fixed. The module takes the current codebook index from the central controller and synchronization signal from an external clock.

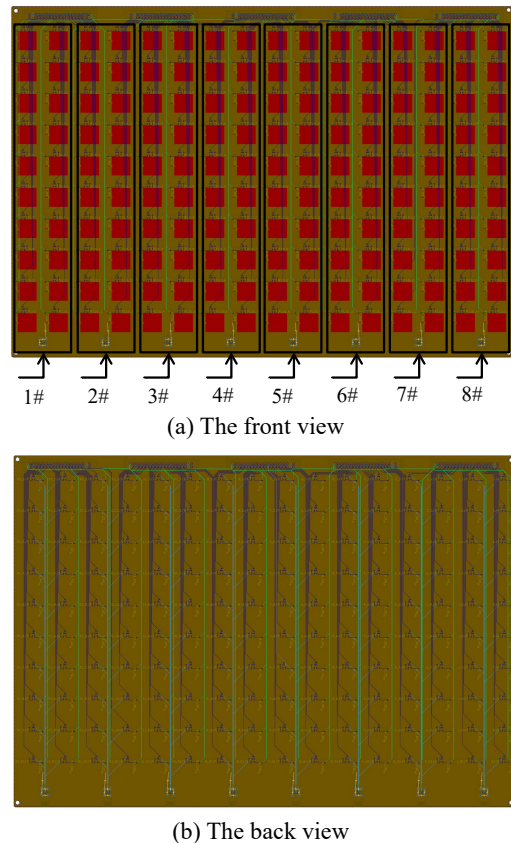


Figure 10. The PCB structure of our decoupled-oriented AWG-RIS prototype. (a) The front view of PCB: the numbers represent the index of input interface where the control signal manipulate the bias voltages of all the units within the corresponding black box. (b) The back view of PCB.

4) *Center Controller*: The center controller is responsible for implementing all algorithms required for waveform calculation and codebook generation across various tasks. Two digital high-speed control signals are output into the signal

generator module and the beamforming module according to the results of the algorithm.

5) *Synchronization Module*: The timing module provides the same reference clock to the center controller module, the signal generator module and the beamforming module.

6) *USRP*: The USRP platform receive the RF signal from the cable connected with the horn antenna, obtain the baseband signal through the down-converter and send the digital baseband to the host computer. Some necessary signal processes are deployed in host computer of the USRP.

7) *Air-fed*: The RF air-fed signal is generated by the vector signal source (Keysight N5186A). In our prototype, the air-fed carrier is the 5.8GHz continuous wave. It is worth noting that in practical applications, a low-cost single-tone RF signal source or the EM wave in the environment can provide this carrier signal instead of the expensive RF signal generator instrument.

C. Experimental Results

As shown in Fig.9 (a), we deployed the prototype in the microwave anechoic chamber that eliminates the interference of environment EM wave. The air-fed horn antenna is approximately 30° to the right of the perpendicular plane of the RIS and at a distance of 50 cm. The receiving antenna is approximately 15° to the left of the perpendicular plane of the RIS and at a distance of 1.5 meters. The purpose of the experiments is to validate the arbitrary waveform generation capability of the AWG-RIS. Therefore, we set up experiments for arbitrary waveform generation and spectrum generation with fixed transmitting and receiving antennas.

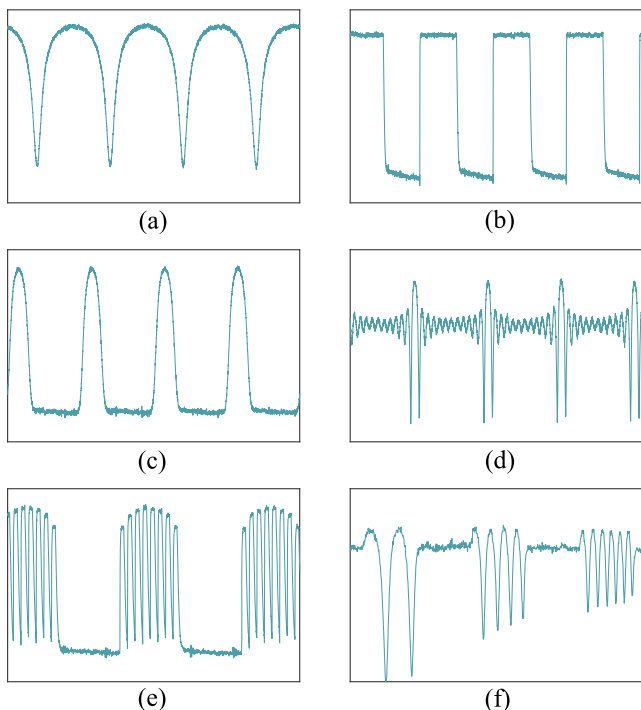


Figure 11. Several waveforms generated by the RIS for a single input signal. (a) the distorted sinusoidal signal; (b) the square wave; (c) the Gaussian Pulse; (d) the sinc function wave; (e) the radar pulse; (f) the frequency modulation symbols.

The received baseband waveforms generated by RIS with the aid of single DAC are shown in Fig.11 where the only

DAC is parallelly connected with all the inputs (1#~8#). We set six common waveforms that are used in communication, radar, and signal processing fields as control signals. These signals underwent responses from the RLC circuit, changes in the voltage-reflection coefficient mapping due to unit non-linearity, and spatial propagation, and were finally received as baseband signals by the horn antenna. As a clear example, the sinusoid wave signal exhibited nonlinear distortion. This distortion mainly originated from the nonlinear voltage-reflection coefficient mapping of the units since a single-frequency signal is not affected by the RLC circuit. The amplitude range of these control signals is set to a low level of 1V and a high level of 5V, with a frequency of 10 kHz (meaning the same waveform repeats every 100 microseconds). After DC filtering, the amplitude of the received signal is approximately 2 dBm.

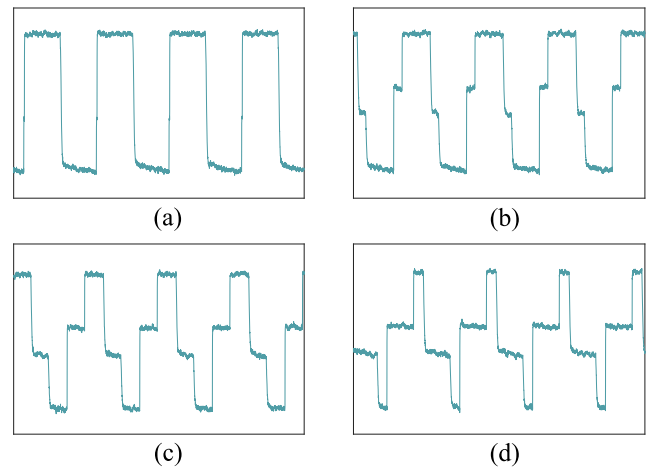


Figure 12. The waveforms that combining two equal 10kHz square-waves with four different initial phases: (a) 0 degree; (b) 45 degree; (c) 90 degree; (d) 135 degree

As shown in Fig.12, two square waves with the same frequency (i.e. 10kHz) and the same amplitude are combined with four initial phase differences, i.e., 0/45/90/135 degrees. Given that the air-fed source is located in the near-field of the RIS, the incident wave should be regarded as a spherical wave. Consequently, the EM wave energy that arrives at each unit of the RIS varies. The two DACs are alternately connected to the 8 inputs, i.e. the first DAC connected with input 1#, 3#, 5# and 7# (the second one connected with the remainder), which keeps the equality of the energy proportion of two control signals. As shown in Fig.13, we obtain the multiple unusual waveforms stemmed from two elementary waveform $x_1(t)$ and $x_2(t)$. The findings confirm that implementing analog control endows the RIS with the capability for both direct generation and multi-input superimposed generation of baseband signals.

Fig.14 shows the spectrum of the received signal generated by the input of eight different frequency sinusoidal signals. Each sinusoidal input signal has the same amplitude, but the energy at each frequency point in the received signal spectrum is not uniform. This is because the incident wave from the feed source cannot be approximated as a plane wave for the RIS. Therefore, an accurate channel model must be considered when synthesizing baseband signal waveforms.

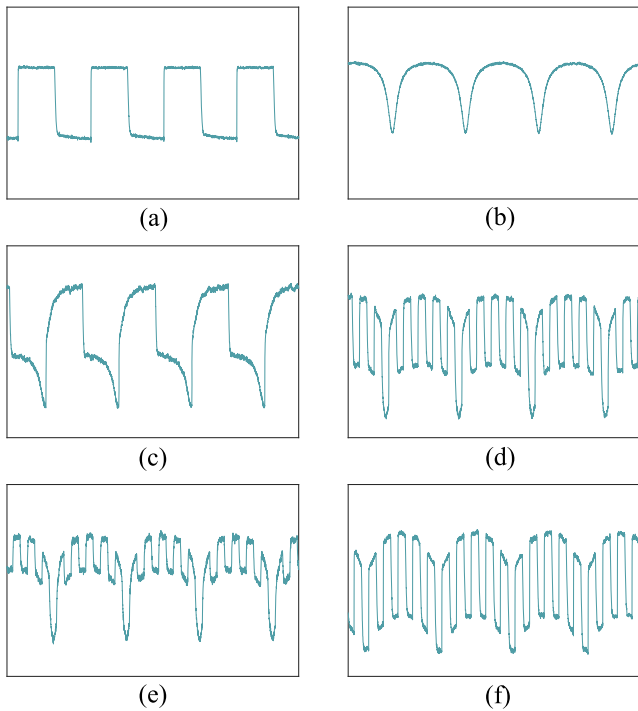


Figure 13. The superposition of two different waveform (i.e., $x_1(t)$ and $x_2(t)$) who suffer from the time-domain scaling and the magnitude scaling. (a) $x_1(t)$; (b) $x_2(t)$; (c) $\frac{1}{2}(x_1(t) + x_2(t))$; (d) $\frac{1}{2}(x_1(5t) + x_2(t))$; (e) $\frac{1}{3}x_1(5t) + \frac{2}{3}x_2(t)$; (f) $\frac{2}{3}x_1(5t) + \frac{1}{3}x_2(t)$

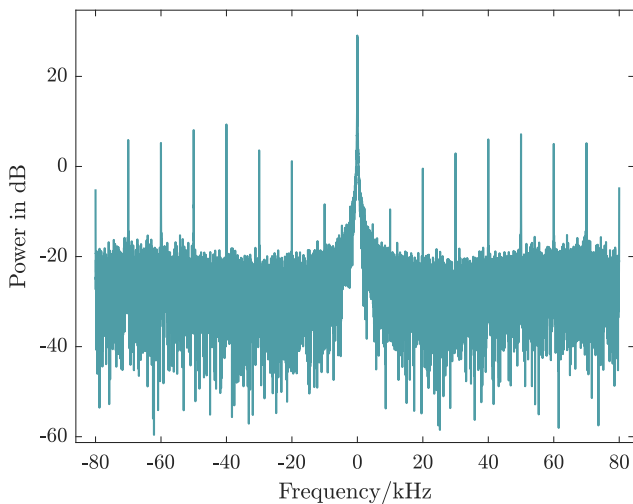


Figure 14. The baseband spectrum of received signal that is generated by eight different inputs which are respectively sinusoidal signal with frequency of 10kHz, 20kHz, 30kHz, 40kHz, 50kHz, 60kHz, 70kHz and 80kHz.

Compared to previous RIS modulation work, where quantized waveforms are generated through phase superposition, resulting in undesirable harmonic components, our proposed framework can produce clean, desired spectrum and waveform.

As shown in Fig.15, we utilized a single input to generate a time-frequency spectrum similar to the desired image. First, we generated the desired image, ensuring that it is vertically symmetrical, as we need to produce a real signal whose

spectrum is symmetric about the $\omega = 0$ axes. The resolution of the desired image should be matched with the number of samples and points of the discrete Fourier transform. The two-dimension image is equivalent to the spectrogram defined in Eq.(21). The control signal is obtained by inverse STFT and Eq.(20). The air-fed source is a monochromatic continuous wave, and the received baseband signal consists of the dc part, noise, and desired signal. After denoising, DC filtering, and other preprocessing steps, the received time domain signal is transformed using STFT, resulting in the spectrogram shown in the last column of Fig.15.

VI. CONCLUSION

In this paper, we have introduced a novel paradigm for AWG-RIS that features a decoupled unit design and a separated functionality control structure, enabling independent generation of continuous waveforms and beam patterns. We have also presented an analytical framework that includes the impulse response of the control circuits and the nonlinear characteristics of diode-based patches. Additionally, we have proposed a new RIS model incorporating the waveform factor, which adds an extra dimension of operation through the use of a few cost-effective DACs. Furthermore, we have detailed our prototype system, which consists of 10×16 1-bit PIN-based units and 8 control signal interfaces. The experimental results demonstrated the capability to arbitrarily create baseband waveforms and spectrograms using a single input and to generate combined outputs from multiple inputs. The positive outcomes highlight the potential of the AWG-RIS in areas such as backscatter communications, radar spoofing, and ISAC. Future research should concentrate on enhancing modulation efficiency and expanding applications.

REFERENCES

- [1] N. Yu and F. Capasso, "Flat optics with designer metasurfaces," *Nat. Mater.*, vol. 13, no. 2, pp. 139–150, 2014.
- [2] L. Liu *et al.*, "Broadband metasurfaces with simultaneous control of phase and amplitude," *Adv. Mater.*, vol. 26, no. 29, pp. 5031–5036, 2014.
- [3] X. Luo, "Subwavelength optical engineering with metasurface waves," *Adv. Opt. Mater.*, vol. 6, no. 7, p. 1701201, 2018.
- [4] T. J. Cui, M. Q. Qi, X. Wan, J. Zhao, and Q. Cheng, "Coding metamaterials, digital metamaterials and programmable metamaterials," *Light: Sci. Appl.*, vol. 3, no. 10, pp. e218–e218, 2014.
- [5] J. Zhao *et al.*, "Programmable time-domain digital-coding metasurface for non-linear harmonic manipulation and new wireless communication systems," *Natl. Sci. Rev.*, vol. 6, no. 2, pp. 231–238, 2019.
- [6] J. Y. Dai, J. Zhao, Q. Cheng, and T. J. Cui, "Independent control of harmonic amplitudes and phases via a time-domain digital coding metasurface," *Light: Sci. Appl.*, vol. 7, no. 1, p. 90, 2018.
- [7] J. Y. Dai *et al.*, "High-efficiency synthesizer for spatial waves based on space-time-coding digital metasurface," *Laser Photonics Rev.*, vol. 14, no. 6, p. 1900133, 2020.
- [8] J. C. Ke *et al.*, "Linear and nonlinear polarization syntheses and their programmable controls based on anisotropic time-domain digital coding metasurface," *Small Struct.*, vol. 2, no. 1, p. 2000060, 2021.
- [9] C. Zhang *et al.*, "Convolution operations on time-domain digital coding metasurface for beam manipulations of harmonics," *Nanophotonics*, vol. 9, no. 9, pp. 2771–2781, 2020.
- [10] J. A. Hodge, K. V. Mishra, and A. I. Zaghlool, "Intelligent time-varying metasurface transceiver for index modulation in 6g wireless networks," *IEEE Antennas Wirel. Propag. Lett.*, vol. 19, no. 11, pp. 1891–1895, 2020.
- [11] W. Tang *et al.*, "Mimo transmission through reconfigurable intelligent surface: System design, analysis, and implementation," *IEEE J. Sel. Areas Commun.*, vol. 38, no. 11, pp. 2683–2699, 2020.
- [12] J. Y. Dai *et al.*, "Realization of multi-modulation schemes for wireless communication by time-domain digital coding metasurface," *IEEE Trans. Antennas Propag.*, vol. 68, no. 3, pp. 1618–1627, 2019.

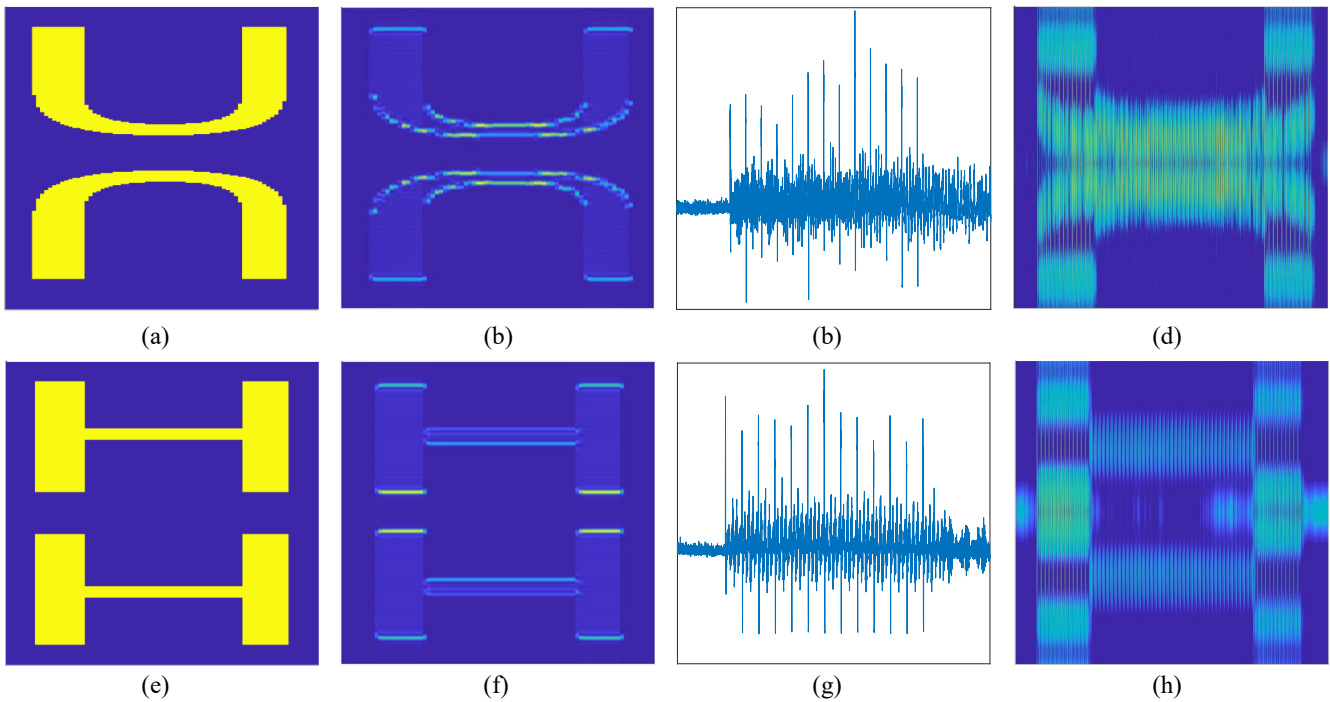


Figure 15. Arbitrary Time-frequency spectrogram Generation. The sub-figures (a) and (e) in the first column are the expected spectrograms (i.e., letter 'U' and 'H'). The subfigures (b) and (f) in the second column are, respectively, the simulated results. The next column includes the received time-domain signals which are respectively generated by inverse STFT. The last column (d) and (h) show the spectrogram of the received signal.

- [13] L. Zhang *et al.*, "Space-time-coding digital metasurfaces," *Nat. Commun.*, vol. 9, no. 1, p. 4334, 2018.
- [14] Z. Yu and S. Fan, "Complete optical isolation created by indirect interband photonic transitions," *Nat. Photonics*, vol. 3, no. 2, pp. 91–94, 2009.
- [15] A. Shaltout, A. Kildishev, and V. Shalaev, "Time-varying metasurfaces and lorentz non-reciprocity," *Opt. Mater. Express*, vol. 5, no. 11, pp. 2459–2467, 2015.
- [16] Y. Hadad, D. L. Sounas, and A. Alu, "Space-time gradient metasurfaces," *Phys. Rev. B*, vol. 92, no. 10, p. 100304, 2015.
- [17] L. Zhang *et al.*, "Dynamically realizing arbitrary multi-bit programmable phases using a 2-bit time-domain coding metasurface," *IEEE Trans. Antennas Propag.*, vol. 68, no. 4, pp. 2984–2992, 2019.
- [18] A. M. Shaltout, V. M. Shalaev, and M. L. Brongersma, "Spatiotemporal light control with active metasurfaces," *Science*, vol. 364, no. 6441, p. eaat3100, 2019.
- [19] H. Rajabalipanah, A. Abdolali, S. Iqbal, L. Zhang, and T. J. Cui, "How do space-time digital metasurfaces serve to perform analog signal processing?" *arXiv preprint arXiv:2002.06773*, 2020.
- [20] Y. Liu *et al.*, "Toward sub-terahertz: Space-time coding metasurface transmitter for wideband wireless communications," *Adv. Sci.*, vol. 10, no. 29, p. 2304278, 2023.
- [21] J. Yao, J. Xu, W. Xu, C. Yuen, and X. You, "Superimposed ris-phase modulation for mimo communications: A novel paradigm of information transfer," *IEEE Trans. Wireless Commun.*, 2023.
- [22] G.-B. Wu *et al.*, "A universal metasurface antenna to manipulate all fundamental characteristics of electromagnetic waves," *Nat. Commun.*, vol. 14, no. 1, p. 5155, 2023.
- [23] Y. He, Y. Cai, H. Mao, and G. Yu, "Ris-assisted communication radar coexistence: Joint beamforming design and analysis," *IEEE J. Sel. Areas Commun.*, vol. 40, no. 7, pp. 2131–2145, 2022.
- [24] H. Ren *et al.*, "Metasurface orbital angular momentum holography," *Nat. Commun.*, vol. 10, no. 1, p. 2986, 2019.
- [25] X. Bai *et al.*, "Dynamic millimeter-wave oam beam generation through programmable metasurface," *Nanophotonics*, vol. 11, no. 7, pp. 1389–1399, 2022.
- [26] J. Hu *et al.*, "Reconfigurable intelligent surface based rf sensing: Design, optimization, and implementation," *IEEE J. Sel. Areas Commun.*, vol. 38, no. 11, pp. 2700–2716, 2020.
- [27] R. Long, Y.-C. Liang, Y. Pei, and E. G. Larsson, "Active reconfigurable intelligent surface-aided wireless communications," *IEEE Trans. Wireless Commun.*, vol. 20, no. 8, pp. 4962–4975, 2021.
- [28] M. H. Khoshafa, T. M. Ngatched, M. H. Ahmed, and A. R. Ndjongue, "Active reconfigurable intelligent surfaces-aided wireless communication system," *IEEE Commun. Lett.*, vol. 25, no. 11, pp. 3699–3703, 2021.
- [29] G. Chen, Q. Wu, C. He, W. Chen, J. Tang, and S. Jin, "Active iris aided multiple access for energy-constrained iot systems," *IEEE Trans. Wireless Commun.*, vol. 22, no. 3, pp. 1677–1694, 2022.
- [30] Z. Zhang *et al.*, "Active ris vs. passive ris: Which will prevail in 6g?" *IEEE Trans. Commun.*, vol. 71, no. 3, pp. 1707–1725, 2022.
- [31] S. Zhang, H. Zhang, B. Di, Y. Tan, Z. Han, and L. Song, "Beyond intelligent reflecting surfaces: Reflective-transmissive metasurface aided communications for full-dimensional coverage extension," *IEEE Trans. Veh. Technol.*, vol. 69, no. 11, pp. 13 905–13 909, 2020.
- [32] J. Xu, Y. Liu, X. Mu, and O. A. Dobre, "Star-riss: Simultaneous transmitting and reflecting reconfigurable intelligent surfaces," *IEEE Commun. Lett.*, vol. 25, no. 9, pp. 3134–3138, 2021.
- [33] A. de Lustrac, B. Ratni, G.-P. Piau, Y. Duval, and S. N. Burokur, "Tri-state metasurface-based electromagnetic screen with switchable reflection, transmission, and absorption functionalities," *ACS Appl. Electron. Mater.*, vol. 3, no. 3, pp. 1184–1190, 2021.
- [34] J. Wang *et al.*, "Transmission–reflection-integrated quadratic phase metasurface for multifunctional electromagnetic manipulation in full space," *Adv. Opt. Mater.*, vol. 10, no. 6, p. 2102111, 2022.
- [35] X. G. Zhang *et al.*, "Polarization-controlled dual-programmable metasurfaces," *Adv. Sci.*, vol. 7, no. 11, p. 1903382, 2020.
- [36] L. Yan *et al.*, "Arbitrary and independent polarization control in situ via a single metasurface," *Adv. Opt. Mater.*, vol. 6, no. 21, p. 1800728, 2018.
- [37] T. Jiang *et al.*, "Backscatter communication meets practical battery-free internet of things: A survey and outlook," *IEEE Commun. Surv. Tutorials*, 2023.
- [38] J. Kimionis, A. Georgiadis, S. N. Daskalakis, and M. M. Tentzeris, "A printed millimetre-wave modulator and antenna array for backscatter communications at gigabit data rates," *Nat. Electron.*, vol. 4, no. 6, pp. 439–446, 2021.
- [39] E. Biglieri, R. Calderbank, A. Constantinides, A. Goldsmith, A. Paulraj, and H. V. Poor, *MIMO wireless communications*. Cambridge university press, 2007.

- [40] H. Taub and D. L. Schilling, "Principles of communication systems," *Singapore*, 1986.
- [41] V. F. Fusco and Q. Chen, "Direct-signal modulation using a silicon microstrip patch antenna," *IEEE Trans. Antennas Propag.*, vol. 47, no. 6, pp. 1025–1028, 1999.
- [42] F. Amato, C. W. Peterson, B. P. Degnan, and G. D. Durgin, "Tunneling rfid tags for long-range and low-power microwave applications," *IEEE J. Radio Freq. Identif.*, vol. 2, no. 2, pp. 93–103, 2018.
- [43] A. Varshney, A. Soleiman, and T. Voigt, "Tunnelscatter: Low power communication for sensor tags using tunnel diodes," in *The 25th annual international conference on mobile computing and networking*, 2019, pp. 1–17.
- [44] R. Reed, F. L. Pour, and D. S. Ha, "An energy efficient rf backscatter modulator for iot applications," in *2021 IEEE International Symposium on Circuits and Systems (ISCAS)*. IEEE, 2021, pp. 1–5.
- [45] X. Guo, Y. He, Z. Yu, J. Zhang, Y. Liu, and L. Shangguan, "Rf-transformer: a unified backscatter radio hardware abstraction," in *Proceedings of the 28th annual international conference on mobile computing and networking*, 2022, pp. 446–458.
- [46] R. Xiong *et al.*, "Multi-RIS-aided Wireless Communications in Real-world: Prototyping and Field Trials," *arXiv e-prints*, p. arXiv:2303.03287, Mar. 2023.
- [47] X. Dong, R. Xiong, T. Mi, Y. Xie, and R. C. Qiu, "Transforming ris-assisted passive beamforming from tedious to simple: A relaxation algorithm for rician channel," *arXiv preprint arXiv:2211.06555*, 2022.